Journal of Alloys and Compounds 509 (2011) 5147–5151

Contents lists available at ScienceDirect

Journal of Alloys and Compounds

journal homepage: www.elsevier.com/locate/jallcom

Raman scattering investigation of Bi_2Te_3 hexagonal nanoplates prepared by a solvothermal process in the absence of NaOH

Yujie Liang[a], Wenzhong Wang[a,b,*], Baoqing Zeng[a], Guling Zhang[b], Jing Huang[b], Jin Li[b], Te Li[b], Yangyang Song[b], Xiuyu Zhang[b]

[a] School of Physical Electronics, University of Electronic Science and Technology of China, Chengdu 610054, China
[b] School of Science, Minzu University of China, Beijing 100081, China

ARTICLE INFO

Article history:
Received 28 December 2010
Received in revised form 31 January 2011
Accepted 1 February 2011
Available online 2 March 2011

Keywords:
Nanostructured materials
Thermoelectric materials
Crystal growth
Crystal structure
Optical spectroscopy

ABSTRACT

Hexagonal Bi_2Te_3 nanoplates were synthesized by a simple solvothermal process in the absence of NaOH. The composition, morphology and size of the as-prepared products were characterized by powder X-ray diffraction (XRD) and transmission electron microscopy (TEM). Raman scattering optical properties of the as-prepared Bi_2Te_3 nanoplates were investigated by micro-Raman spectroscopy. The Raman spectrum shows that infrared (IR) active mode (A_{1u}), which must be odd parity and is Raman forbidden for bulk crystal due to its inversion symmetry, is greatly activated and shown up clearly in Raman scattering spectrum. We attribute the appearance of infrared active (A_{1u}) in Raman spectrum to crystal symmetry breaking of Bi_2Te_3 hexagonal nanoplates. The as-grown Bi_2Te_3 hexagonal nanoplates, exhibiting novel Raman optical properties compared with bulk crystals, may find potential applications in thermoelectric devices.

1. Introduction

Bismuth telluride (Bi_2Te_3), an important V–VI semiconductor with a band gap of 0.15–0.2 eV [1–4], is the most important thermoelectric (TE) material that operates near the room temperature [5–8]. Therefore the synthesis of Bi_2Te_3 nanostructures with controllable morphology and size has attracted considerable attention for many years. Till date, various methods have been employed to prepare Bi_2Te_3 nanostructures [9–17]. Among these synthetic methods, hydrothermal/solvothermal method, which is a simple and convenient chemical route without the need of high synthetic temperature and costly devices, has been generally employed to synthesize Bi_2Te_3 nanostructures with various morphologies and sizes, such as nanorods, nanowires, sheets, hexagonal nanoplates, rode-like and flower-like nanostructures.

Bi_2Te_3 has a rhombohedral geometry with the space group D^5_{3d} ($R\bar{3}m$) [18]. The atomic arrangement in Bi_2Te_3 crystal structure can be better visualized in terms of the layered structure, in which each charge neutralized layer is built up by five covalently bonded monatomic sheets, defined as *quintuple* layers, along the C_H axis with the sequence $Te^{(1)}$–Bi–$Te^{(2)}$–Bi–$Te^{(1)}$ (see Fig. 1). The quintuple layers are weakly bound to each other by the van der Waals interaction to form the crystal. The band gap in a single quintuple is larger than in a few-quintuple layer (FQL) because the latter has less coupling between the surface states of the top and bottom interfaces. The presence of the van der Waals gap between the quintuples results in preferential cleavage plane between the outmost adjacent $Te^{(1)}$ layers in the sequence of $Te^{(1)}$–Bi–$Te^{(2)}$–Bi–$Te^{(1)}$. The superscripts (1) and (2) denote two different chemical states of Te anions. These anisotropic crystallography features make it possible to fabricate Bi_2Te_3 nanostructures with sheet-like morphology. In this article, we employed a simple solvothermal process to prepare Bi_2Te_3 hexagonal nanoplates in the absence of NaOH. The as-prepared nanoplates were characterized by X-ray diffraction (XRD), transmission electron microscope (TEM), high resolution TEM (HRTEM) and Raman spectroscopy. The Raman spectrum shows that infrared (IR) active mode (A_{1u}), which must be odd parity and is Raman forbidden for bulk crystal due to its inversion symmetry, is greatly activated and shown up clearly in Raman scattering spectrum, resulting from crystal symmetry breaking of Bi_2Te_3 hexagonal nanoplates.

2. Experimental procedure

In this work, all chemicals were used as received without further purification. In all experiments, Bi_2O_3 and Te powder were used as starting materials and the molar ratio of Bi:Te was adopted to 2:3, ethylene glycol was used as both solvent and reducing agent, polyvinylpyrrolodone (PVP) was used as stabilizing agent. A typical procedure for the solvothermal synthesis of Bi_2Te_3 nanoplates is given as fol-

* Corresponding author at: School of Science, Minzu University of China, 27 South Zhongguancun Street, Beijing 100081, China. Tel.: +86 10 68930239; fax: +86 10 68930239.
E-mail address: wzhwang@aphy.iphy.ac.cn (W. Wang).

0925-8388/$ – see front matter © 2011 Elsevier B.V. All rights reserved.
doi:10.1016/j.jallcom.2011.02.015

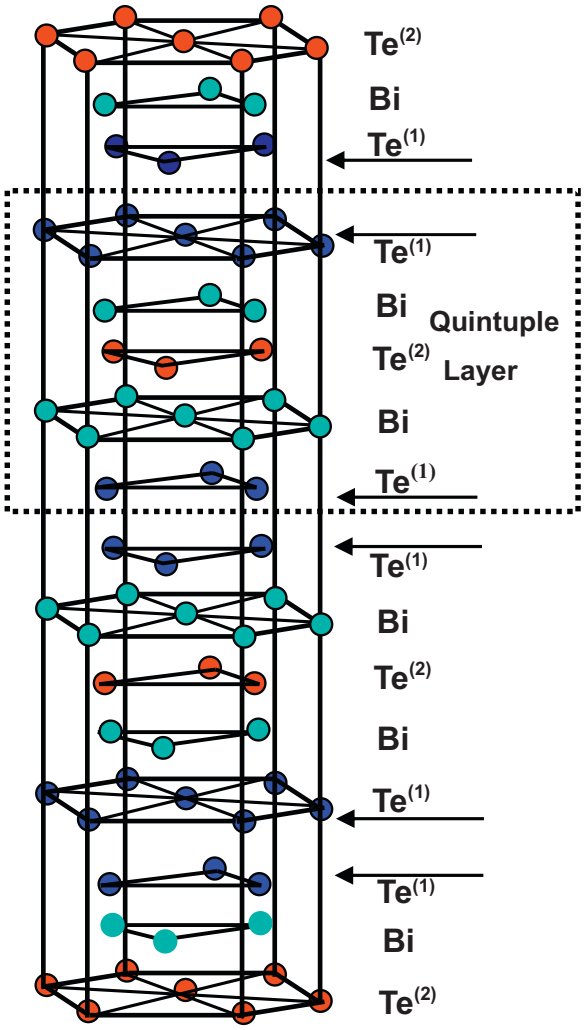

Fig. 1. Schematic of Bi_2Te_3 crystal structure with each quintuple layer (QL) formed by five Bi and Te atomic sheets.

lows: 0.4 g PVP (K-30) was dissolved in 20 mL ethylene glycol (spectrophotometric grade, 99+%) to form a clear solution with the help of continuous magnetic stirring, then 0.5 mmol Bi_2O_3 (analytical grade) and 1.5 mmol tellurium powder (99.99%) were added to the solution. The mixtures were stirred vigorously for 30 min and then transferred into a 50-mL Telfon-lined stainless-steel autoclave, sealed, kept at 200 °C in a furnace for 12 h, and cooled to room temperature. The precipitates were centrifuged, filtered, washed with distilled water and absolute ethanol for several times, and finally dried in an oven at 60 °C for 12 h in air.

The phase structure of the as-prepared products was investigated by X-ray diffraction (XRD) with a Pgeneral XD-3 diffractometer with Cu Kα radiation (λ = 1.54056 Å) being the excitation source at 36 kV, 20 mA. The morphology and size of the products were observed by transmission electron microscopy (JEM 2010), with an accelerating voltage of 200 kV. Raman spectra were recorded on a LabRam HR800 confocal microprobe Raman system (Jobin-Yvon). The excitation line was 632.8 nm from a He–Ne laser.

3. Results and discussion

The chemical composition and phase structure of the as-prepared Bi_2Te_3 nanoplates were first studied by XRD. Fig. 2 is a XRD pattern of the as-grown nanoplates. All diffraction peaks in the XRD pattern can be indexed to Bi_2Te_3 rhombohedral lattice phase with the reported lattice constants $a = 4.395$ and $c = 30.44$ Å (JCPDS Card Number 82-0358). Six main peaks can be easily indexed to (0 1 5), (1 0 1 0), (1 1 0), (2 0 5), (0 2 1 0) and (1 1 1 5) planes of Bi_2Te_3 rhombohedral lattice phase. The shoulder of the main peak (0 1 5) of can be indexed to (0 1 2) plane of Bi (JCPDS Card Number 85-1331). No peaks of Te and other alloy compounds were detected.

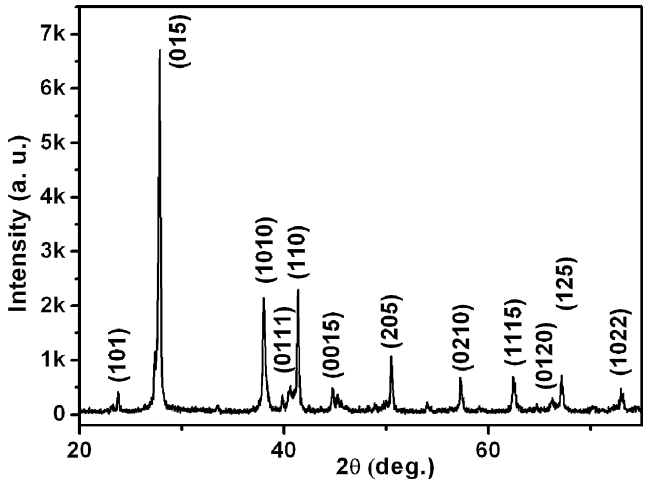

Fig. 2. XRD pattern of Bi_2Te_3 hexagonal nanoplates synthesized by a solvothermal process in the absence of NaOH.

Thus the XRD data indicates that Bi_2Te_3 nanoplates prepared via present method is composed of Bi_2Te_3 rhombohedral lattice phase.

The typical TEM images of the as-prepared Bi_2Te_3 nanostructures are shown in Fig. 3. TEM image indicates that that most of the as-prepared products are hexagonal nanoplates with edge lengths of about 1.5–5 μm as shown in Fig. 3a. Fig. 3b is a typical TEM image of a single nanoplate, clearly demonstrating that the nanoplate has perfect hexagonal morphology. One also can find some nanoplates exhibit the truncated hexagonal morphology as presented in Fig. 3c. It is worth noting that some nanoplates are almost transparent under the electron beam since copper grid below the nanoplate can be seen clearly as shown in Fig. 3d, meaning that the as-grown nanoplates are very thin. Careful TEM examinations show that the percentage of the transparent nanoplates in the sample is about 55%.

The microstructure and crystallinity of the as-prepared hexagonal nanoplates were further investigated by high-resolution TEM (HRTEM). Fig. 4a shows the TEM image of a single hexagonal Bi_2Te_3 nanoplate used to make a detailed investigation of crystallinity and microstructure. Corresponding spot pattern of SAED (insert of Fig. 4a) and HRTEM lattice shown in Fig. 4b, demonstrate the single crystalline nature of the nanoplate. The SAED (insert of Fig. 4a) pattern was obtained by aligning the electron beam perpendicular to the face of this plate. The hexagonally symmetric spot pattern indicates the single crystallinity, and can be indexed based on a rhombohedral cell with lattice parameter of $a = 4.395$ and $c = 30.44$ Å. An HRTEM image (Fig. 4b) reveals expected hexagonal lattice fringes with a lattice spacing of 0.223 nm, indicating that the as-prepared nanoplates are highly crystallized. The spacing is about 0.223 nm, consistent with the lattice spacing of $(1\,1\,\bar{2}\,0)$ planes of the Bi_2Te_3. The result indicates that growth direction for developing the truncated hexagonal Bi_2Te_3 nanoplates is $(1\,1\,\bar{2}\,0)$, which is consistent with the previous report [14]. Since the nanoplates grew along $\langle 1\,1\,\bar{2}\,0\rangle$ direction and have the hexagonal outline, it is reasonable to say that the nanoplates are normal to $\langle 0\,0\,0\,1\rangle$ direction, i.e. the nanoplates have large $(0\,0\,0\,1)$ faces and are bounded by $\langle 1\,1\,\bar{2}\,0\rangle$ faces on the six edges, and the growth direction for developing the hexagonal nanoplates is $\langle 1\,1\,\bar{2}\,0\rangle$ direction, which is in good agreement with the previous published literature [14].

Raman spectroscopy, which is a sensitive probe to the local atomic arrangements and vibrations of the materials, has been widely used to investigate the microstructure of the nano-sized materials [19–24]. Before discussing Raman optical properties of Bi_2Te_3 nanoplates, we first discuss the crystal structure of

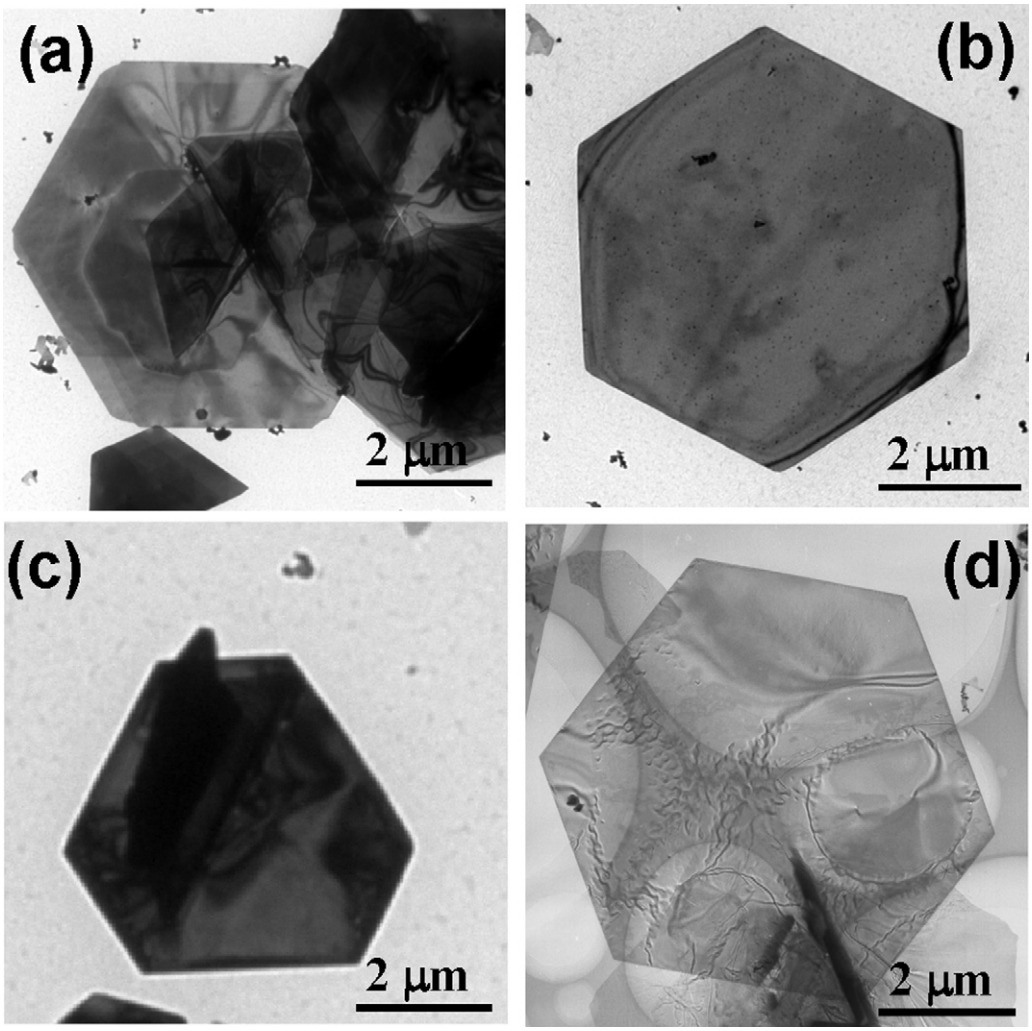

Fig. 3. (a) TEM images of Bi_2Te_3 nanoplates, showing hexagonal shape. (b) TEM image of a single perfect hexagonal nanoplate. (c) TEM image of a single truncated hexagonal nanoplate. (d) TEM image of a single hexagonal nanoplate, showing its thickness is very thin.

Bi_2Te_3 crystal. It was reported that bulk Bi_2Te_3 crystal belongs to the space group $D^5{}_{3d}$ ($R\bar{3}m$) with five atoms in per primitive cell [18]. Consequently, bulk crystals exhibit 15 lattice vibration modes due to inversion symmetry. Three of these vibration modes are acoustic and twelve are optical phonons. The group theory classification rules that 12 optical modes are characterized by $2A_{1g} + 2E_g + 2A_{1u} + 2E_u$ [25]. These phonon modes are exclusively either Raman or infrared (IR) active [25] because of the inversion

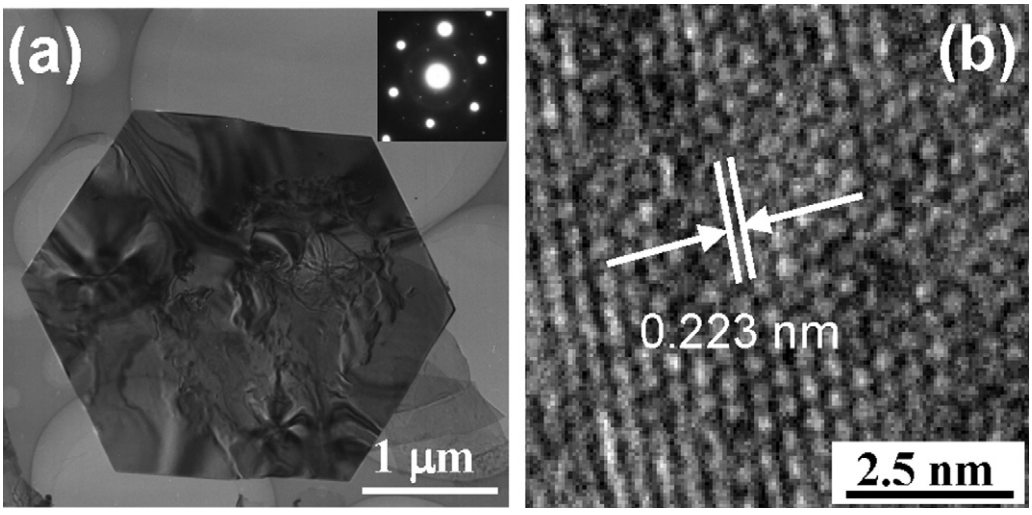

Fig. 4. (a) TEM image of a single hexagonal Bi_2Te_3 nanoplate used to make investigations of crystallinity and microstructure. SAED pattern (insert of a) and (b) HRTEM image of nanoplate of (a), showing a highly crystal nature of the as-prepared nanoplates.

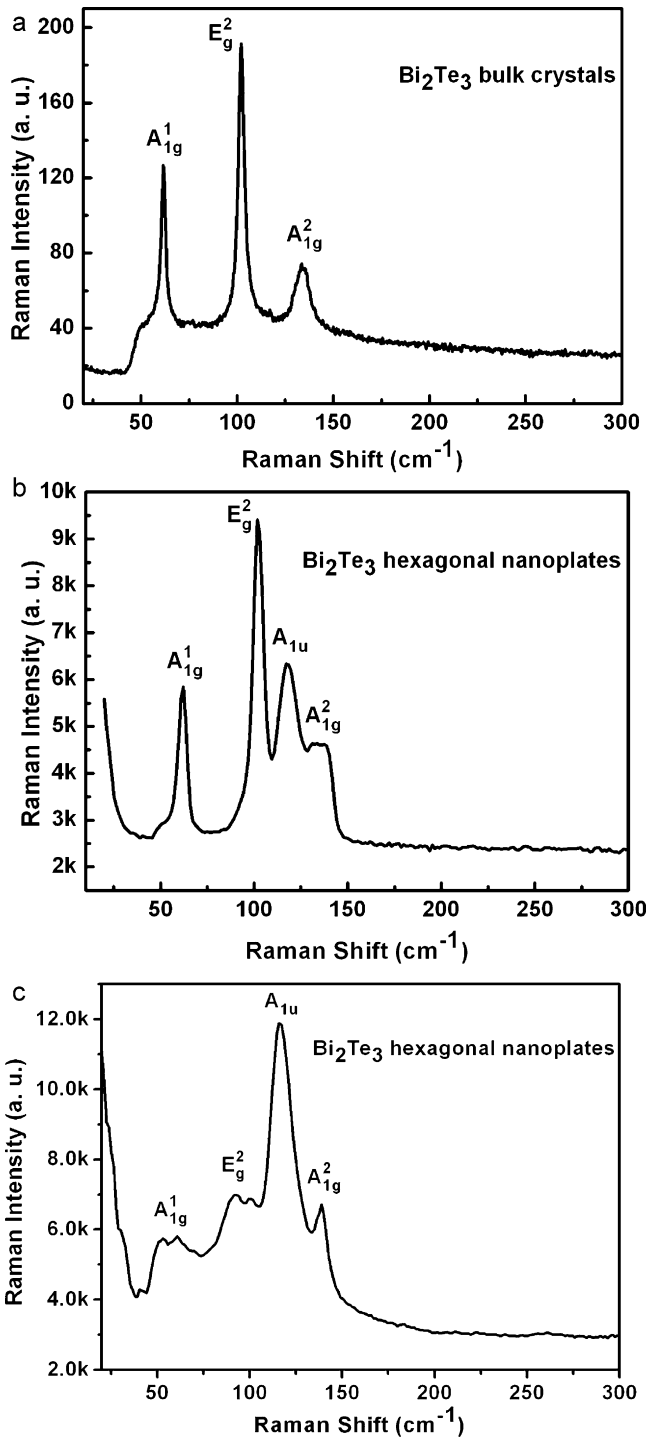

Fig. 5. Raman scattering spectra of (a) as-bought Bi_2Te_3 bulk crystals, and (b and c) as-prepared hexagonal Bi_2Te_3 nanoplates.

symmetry of the crystal. While both A_{1g} and E_g modes are 2-fold degenerate. The atoms vibrate in-plane and out-of-plane in these phonon modes. In E_g modes, the atoms vibrate in the basal plane, while in A_{1g} modes, the atoms vibrate along C_H. Due to inversion symmetry of crystals, the IR-active modes (A_{1u}) must be odd parity, while the Raman-active modes (E_g, A_{1g}) must be even parity under inversion [26]. The odd-parity IR active phonon modes are Raman forbidden and do not show up in Raman spectra for bulk crystals with crystal symmetry.

Now we turn to the analysis of Raman spectra of the Bi_2Te_3 nanoplates. The Raman scattering spectrum of the as-prepared Bi_2Te_3 thin hexagonal nanoplates with edge lengths of about 1.5–5 μm is shown in Fig. 5b. The Raman scattering spectrum of bulk Bi_2Te_3 crystals with size of about 10–20 μm is also given as shown in Fig. 5a for comparison. The Raman spectrum of bulk crystals exhibit three Brillouin zone (BZ) center Raman active modes at 61, 102 and 134 cm^{-1}. Three Raman optical phonon peaks can be identified as $A_{1g}{}^1$ at 61 cm^{-1}, $E_g{}^2$ at 102 cm^{-1}, and $A_{1g}{}^2$ at 134 cm^{-1}. The peak positions are very close to the previously measured and assigned Raman peaks of bulk crystalline Bi_2Te_3 [27,28]. In Raman spectrum of the thin hexagonal nanoplates, there Raman peaks are also located at 61, 102 and 134 cm^{-1}, respectively. The peak positions are same as the measured and assigned Raman peaks of above bulk crystalline Bi_2Te_3.

However, one can find a very interesting result that an additional peak with obvious intensity appears at ~119 cm^{-1} in Raman spectrum of the thin nanoplates (Fig. 5b). This peak is identified as A_{1u} mode composed of longitudinal optical (LO) phonons at the BZ boundary (Z point). The A_{1u} mode is IR active mode but not Raman active mode in bulk Bi_2Te_3 crystals [29]. The previous research indicated that the identified crystal symmetry breaking is likely related to the loss of infinite crystal periodicity owing to interfaces and corresponding relaxation of the phonon wave vector $q = 0$ selection rule. We therefore can reasonably attribute the appearance of IR active A_{1u} mode in thin hexagonal nanoplates to the crystal symmetry breaking of nanoplates due to the presence of two interfaces. Thus the Raman measurements of the as-grown thin nanoplates unambiguously demonstrate that infrared (IR) active mode (A_{1u}), which must be odd parity and is Raman forbidden for bulk crystal due to its inversion symmetry [26], is activated and shown up in Raman scattering spectra, showing the crystal symmetry breaking of the as-prepared Bi_2Te_3 thin square nanoplates.

Further investigations indicate that some nanoplates exhibit the strongest A_{1u} peak in Raman spectrum. Fig. 5c shows a typical micro-Raman scattering spectrum obtained from another micro-area of the nanoplates with edge lengths of about 1.5–5 μm, clearly showing the strongest A_{1u} peak. We attribute appearance of the strongest A_{1u} peak to the crystal symmetry breaking of nanoplates with very thin thickness. Thus Raman spectra indicate that the thickness of as-prepared nanoplates is not uniform. This result can be verified by our above TEM observations, in which some nanoplates are not transparent to electron beam (see Fig. 3b) and others are transparent to electron beam just as shown in Fig. 3d. Thus the Raman spectra of the as-prepared Bi_2Te_3 hexagonal thin nanoplates unambiguously demonstrate the crystal symmetry breaking of the nanoplates.

4. Conclusions

In summary, we synthesized hexagonal Bi_2Te_3 nanoplates by using a simple solvothermal process in the absence of NaOH. Powder X-ray diffraction (XRD) and transmission electron microscopy (TEM) were first used to characterize the composition, morphology and size of the as-prepared products. We employ micro-Raman scattering spectroscopy to investigate the Raman scattering optical properties of the as-prepared Bi_2Te_3 hexagonal nanoplates in detail. The Raman spectrum shows that infrared (IR) active mode (A_{1u}), which must be odd parity and is Raman forbidden for bulk crystal due to its inversion symmetry, is greatly activated and shown up clearly in Raman scattering spectrum. The appearance of infrared active (A_{1u}) in Raman spectrum can be attributed to crystal symmetry breaking of Bi_2Te_3 hexagonal nanoplates due to the presence of two interfaces. The as-grown Bi_2Te_3 hexagonal nanoplates, showing novel Raman optical properties compared with bulk crystals, may find potential applications in thermoelectric devices.

Acknowledgments

This work was supported by the National Natural Science Foundation of China (NSFC, Grant Nos. 11074312, 60071043), the Fundamental Research Funds for the Central Universities (No. 0910KYZD04), "985 project" and "211 project" of Ministry of Education of China, Doctor Station Foundation of the Ministry of Education of China (Grant No. 200806140007), Ministry of Personnel of the People's Republic of China (No. [2007] 170), Ministry of Education of the People's Republic of China (No. [2008] 890), and Undergraduate Research Training Program of Minzu University of China (URTP 200910046) (No. 201011037).

References

[1] C.Y. Li, A.L. Ruoff, C.W. Spencer, J. Appl. Phys. 32 (1961) 1733.
[2] H.J. Goldsmid, Thermoelectric Refrigeration, Plenum Press, New York, 1964.
[3] B.M. Goltsman, B.A. Kudinov, I.A. Smirnov, Thermoelectric Semiconductor Materials Based on Bi_2Te_3, Nauka, Moscow, 1972.
[4] W. Kullmann, J. Geurts, W. Richter, N. Lehner, H. Rauh, U. Steigenberger, G. Eichhorn, R. Geick, Phys. Stat. Sol. B 125 (1984) 131.
[5] L.D. Hicks, M.S. Dresselhaus, Phys. Rev. B 47 (1993) 12727.
[6] L.D. Hicks, M.S. Dresselhaus, Phys. Rev. B 47 (1993) 16631.
[7] T.M. Tritt, Science 283 (1999) 804.
[8] D.Y. Chung, T. Hogan, P. Brazis, M. Rocci-Lane, C. Kannewurf, M. Bastea, C. Uher, M.G. Kanatzidis, Science 287 (2000) 1024.
[9] H.T. Zhang, X.G. Luo, C.H. Wang, Y.M. Xiong, S.Y. Li, X.H. Chen, J. Cryst. Growth 265 (2004) 558.
[10] J.R. Ota, P. Roy, S.K. Srivastava, R. Popovitz-Biro, R. Tenne, Nanotechnology 17 (2006) 1700.
[11] J.H. Zhou, C.G. Jin, J.H. Seol, L. Shi, Appl. Phys. Lett. 87 (2005) 133109.
[12] F. Xiao, B. Yoo, K.H. Lee, N.V. Myung, J. Am. Chem. Soc. 129 (2007) 10068.
[13] Y. Jiang, Y.J. Zhu, J. Cryst. Growth 306 (2007) 351.
[14] G.Q. Zhang, W. Wang, X.L. Lu, X.G. Li, Cryst. Growth Des. 9 (2009) 145.
[15] M. Salavati-Niasari, M. Bazarganipour, F. Davar, J. Alloys Compd. 489 (2010) 530.
[16] G.R. Li, F.L. Zheng, Y.X. Tong, Cryst. Growth Des. 8 (2008) 1226.
[17] Y. Deng, C.W. Nan, N.L. Zhang, T.H. Ji, Q.L. Yang, L. Guo, Solid State Commun. 138 (2006) 111.
[18] W. Kullmann, J. Geurts, W. Richter, N. Lehner, H. Rauh, U. Steigenberger, G. Eichhorn, G. Reick, Phys. Stat. Sol. B 125 (1984) 131.
[19] I.H. Campbell, P.M. Fauchet, Solid State Commun. 58 (1986) 739.
[20] M. Yoshikawa, Y. Mori, H. Obata, M. Maegawa, G. Katagira, H. Ishida, Appl. Phys. Lett. 67 (1995) 694.
[21] Z. Jian, H. IBuscher, C. Falter, W. Ludwig, K. Zhang, X. Xie, Appl. Phys. Lett. 69 (1996) 200.
[22] G.W. Graham, W.H. Wfber, C.R. Peters, R. Vsmen, J. Catal. 130 (1991) 310.
[23] W.Z. Wang, L. Ao, Cryst. Growth Des. 8 (2008) 358.
[24] W.Z. Wang, Y. Zhuang, L. Li, Mater. Lett. 62 (2008) 1014.
[25] W. Richter, C.R. Becker, Phys. Stat. Sol. B 84 (1977) 619.
[26] P.Y. Yu, M. Cardona, Fundamentals of Semiconductors Physics and Materials Properties, Springer, 2005.
[27] V. Russo, A. Bailini, M. Zamboni, M. Passoni, C. Conti, C.S. Casari, A. Bassi, C.E. Bottani, J. Raman Spectrosc. 39 (2008) 205.
[28] L.M. Goncalves, C. Couto, P. Alpuim, A.G. Rolo, F. Völklein, J.H. Correia, Thin Solid Films 518 (2010) 2816.
[29] V. Wagner, G. Dolling, B.M. Powell, G. Landweher, Phys. Stat. Sol. B 85 (1978) 311.